

Theoretical Chemistry Accounts

Surface-dependent properties of α -Ag₂WO₄: a joint experimental and theoretical investigation

--Manuscript Draft--

Manuscript Number:	TCAC-D-20-00072R1	
Full Title:	Surface-dependent properties of α -Ag ₂ WO ₄ : a joint experimental and theoretical investigation	
Article Type:	S.I. : Festschrift in honor of Fernando R. Ornellas	
Keywords:	α -Ag ₂ WO ₄ ; Morphology; Antibacterial activity; Photocatalytic activity.	
Corresponding Author:	Juan Andres, Ph.D. Universitat Jaume I SPAIN	
Corresponding Author Secondary Information:		
Corresponding Author's Institution:	Universitat Jaume I	
Corresponding Author's Secondary Institution:		
First Author:	Leticia O. Laier	
First Author Secondary Information:		
Order of Authors:	Leticia O. Laier	
	Marcelo Assis	
	Camila Cristina De Foggi	
	Amanda Fernandes Gouveia	
	Carlos Eduardo Vergani	
	Luís Carlos Leal Santana	
	Laecio S. Cavalcante	
	Juan Andres, Ph.D.	
	Elson Longo	
Order of Authors Secondary Information:		
Funding Information:	Fundação de Amparo à Pesquisa do Estado de São Paulo (2013/07296-2)	Dr. Elson Longo
	Fundação de Amparo à Pesquisa do Estado de São Paulo (2014/14171-4)	Dr. Elson Longo
	Fundação de Amparo à Pesquisa do Estado de São Paulo (2017/13008-0)	Dr. Elson Longo
	Fundação de Amparo à Pesquisa do Estado de São Paulo (2017/12594-3)	Dr. Camila Cristina De Foggi
	Conselho Nacional de Desenvolvimento Científico e Tecnológico (150949/2018-9)	Dr. Amanda Fernandes Gouveia
	Universitat Jaume I (UJI-B2019-30)	Dr. Juan Andres
	Generalitat Valenciana (PrometeoII/2014/022)	Dr. Juan Andres
	Generalitat Valenciana (ACOMP/2014/270)	Dr. Juan Andres

	Generalitat Valenciana (ACOMP/2015/1202)	Dr. Juan Andres
	Ministerio de Economía y Competitividad (CTQ2015-65207-P)	Dr. Juan Andres
	Ministerio de Ciencia, Innovación y Universidades (PGC2018-094417-B-I00)	Dr. Juan Andres
Abstract:	<p>α-Ag₂WO₄ has attracted much attention in recent years due to its unique crystal and electronic structures, which are suitable for a wide range of applications. This work presents a more realistic study, based on first-principles calculations and experimental results, of the potential of α-Ag₂WO₄ for antibacterial and photocatalytic activity. α-Ag₂WO₄ material has been successfully synthesized by a coprecipitation method and subjected to microwave irradiation for different times. The as-synthesized microcrystals were structurally characterized by X-ray diffraction, while the morphological aspects were investigated by field emission scanning electron microscopy. The experimental studies and theoretical simulations of α-Ag₂WO₄, based on density functional theory calculations, have highlighted several key parameters (surface-dependent) that determine the antibacterial (against <i>Staphylococcus aureus</i>) and photocatalytic activity (for the degradation of Rhodamine B), and provided some general principles for materials design. We believe that our results offer new insights regarding the local coordination of superficial Ag and W cations (i.e. clusters) on each exposed surface of the corresponding morphology, that dictate the antibacterial and photocatalytic activities of α-Ag₂WO₄, a field that has so far remained unexplored.</p>	
Response to Reviewers:	<p>Manuscript ID: TCAC-D-20-00072</p> <p>Response to reviewers</p> <p>We acknowledge the Reviewers for their help in improving our manuscript. As can be seen in the revised text, these comments, remarks and suggestions were considered during our revision. Detailed responses, point-by-point, to the reviewers are summarized below and the changes were made along the revised version of the manuscript and were highlighted in red color.</p> <p>Reviewer #1: The surface-dependent reactivity with respect to the antibacterial and photocatalytic activity is discussed based on the α-Ag₂WO₄ NCs. The authors used their previous theoretical calculations on the α-Ag₂WO₄ to further discuss the surface-dependent properties of these materials including new experimental data. They used the antibacterial and photocatalytic activity to infer about the surface properties of NCs synthesized using different time exposure to microwaves.</p> <p>The manuscript is well written providing an excellent discussion about the surface-dependent properties of α-Ag₂WO₄ and I recommend for publication after the authors address the concerns below.</p> <p>1) The Table 1 and Figure 2 show a correlation between the exposure time to the microwaves and the polyhedron energy. It is well known that the morphologies can be changed with respect to the chemical potential and additives that stabilize one surface with respect to the other. However, the authors just explicit "The theoretical morphologies inserted in the polyhedron energy profile (fig 2) are calculated using the average experimental values of the width and length distribution of the crystals" (page 11, lines 33-35). In my point of view, this is ambiguous, since the proportion of (001) and (101) surfaces could change for the same value of width and length. In my point of view, the values should also be coherent from the thermodynamics point of view. Larger exposure time of microwave should lead to more stable structure (smaller E_{polyhedron}). In my point of view, the authors should clarify this point.</p> <p>Answer: The relative growth rate of each crystal surface along the synthesis process is linked to the appearance and/or disappearance of the exposed surfaces and depends on environmental conditions. These transformations are due to the geometric constraints imposed by the crystal structure and are associated with the relative values of the surface energy among the different of surfaces. In our methodology we calculated the surface energies values associating with the Wulff construction to obtain the complete set of available morphology that a given material can be displayed. We agree with the Reviewer's comment when he said that the values should also be coherent from the thermodynamics point of view. However, our focus here is justly</p>	

demonstrate that through a simple methodology, that correlates the surface energy calculations with the Wulff construction, it is possible to obtain important information about the morphology of the samples, once that the properties of the materials are shape-dependent. Therefore, a note of caution is included in the revised version of the manuscript (see first paragraph of the section 2.1 Computational methods and model systems).

2) Please, include at the Electronic Supplementary Material information about the protocol used to perform the calculations and details of the slab models used (size, number of layers used, etc.) to avoid that the reader to go to the ref. [43] to get that information.

Answer: In the revised version, the protocol used to perform the calculations and details of the slab models used (size, number of layers used, etc.) was included in the Supporting Information (see section SI-2 Computational methods).

Reviewer #2: The manuscript deals with the combined theoretical and experimental study of silver tungstate semiconducting material (alpha polymorph, AWO). The work showed how theoretical methods based on density functional theory (DFT) calculations can help in the conducting and controlled material synthesis and design. Particularly, in the work the AWO microcrystals were synthesized, and treated by microwave irradiation to show how such treatment can affect antibacterial and photocatalytic activity. Combining DFT calculations and knowledge about the morphology of microcrystals the authors explained activity of the dominant surfaces determining the overall shape of microcrystals. The experiments with *Staphylococcus aureus* and Rhodamine B showed that tuning microwave irradiation can lead to optimizing antibacterial activity and photocatalytic degradation. The work brings new knowledge about structural details and active sites of the AWO surfaces. Generally, the manuscript is well organized, the used methods are adequate and the achieved results accompanied with plausible discussion and interpretation. I have following comments and suggestions.

Microwave irradiation - control crystal growth - shape - morphology stays -rod-like hexagonal shape with - controlled but length less (fig. 1)

Answer: The time of microwave irradiation controls both the morphology and the size, as it is displayed in Figure 1

-Figure 2 shows the overall energy of AWO polyhedra with respect to time of irradiation - why is there a significant anomaly for the time 4 mins?

Answer: This anomaly can be associated to the fact that the sample obtained at $t = 4$ min, a destabilization of the (010) surface with concomitant increase of the $E_{\text{polyhedron}}$ value is sensed. In the revised version of the manuscript (see paragraph 1, page 11) this fact is now included.

-In Table 1 a contribution of surface energy of three surfaces to overall polyhedral energy is shown. While for the (001) and (101) surfaces the energy variation is in a reasonable range, for the (010) surface is a very large difference in values for 8 and 16 mins comparing to CP and 2/4 mins irradiation. Is this correct? If yes, why is there such big difference?

Answer: The modulation of the morphologies from experimental results is based on the width and length values from the distribution size of the particles. The width is governed by the (010) surface, while the length is derived from the surface energies values of the (001) surface. Therefore, the ratio between width and length values is the same between the (010) and (001) surfaces. To maintain the rod-like morphology, the ratio between the values of the energy surface of both surfaces needs to be constant; therefore, the surface energy values of (101) surface are not modified. With the increase of the microwave irradiation time, the rod-like morphology suffers an elongation. This elongation is due to the increase of the (surface energy value for the (001) surface, and in order to compensate this increase, the surface energies of (010) need to be stabilized, i.e., its values decrease drastically (from 0.93 to 0.10 eV). However, in general, the percentage of contribution of (010) surface is almost equal in all morphologies (around 15%).

-In the manuscript no details are given about DFT method and parameters of used periodic slabs in calculations of surface energies. In this context, the manuscript refers

to the previous work (ref. 43). Indeed, for the easier orientation of a potential reader, I recommend to add these details to the present manuscript as well. Also information about magnetic state of AWO slabs is missing.

Answer: As we write previously in the question 2 of the reviewer 1, in the revised version, the protocol used to perform the calculations and details of the slab models used (size, number of layers used, etc.) was included in the Supporting Information (see SI-2 Computational methods). With respect to magnetic behavior of AWO, this point is out of the main goal of present work. In future analysis, the corresponding spin densities of the exposed surfaces (at the morphologies), i.e. the magnetic state, will be considered.

-The authors explain the surface activity by a presence of electron-hole (e-h) pairs at surfaces as a consequence of defected sites (incomplete Ag/W coordination, deformed polyhedral units). How these defects are stable with respect to e.g. interaction with water molecules? Is there a study about that?

Answer: In our work, the presence of defect sites is associated to the incomplete Ag/W coordination, deformed polyhedral units. These defects provoke instability and are responsible of the generation of very reactive species with radical behavior, i.e. presence of oxygen vacancies, unpaired electrons, etc. Therefore, these defects are the active sites where the reaction with water molecules, for example, takes place. In the present experimental/theoretical work this innovative mechanism is proposed (see last paragraph of section 3.2 Antibacterial and photocatalytic activity and conclusions section).

-For better understanding of reactivity of surface sites electronic structure (density of states and band gaps) of different surface models could be useful. Did the authors performed an analysis of the electronic structure of the surface slab models?

Answer: The band gaps of different surface models were previously reported. The density of states was analyzed for the set of surfaces presented in the morphologies. The undercoordinated clusters of Ag and W atoms on the top of each surface were analyzed in the manuscript. In the revised Supporting Information (see section SI-3.4 Theoretical analysis of the surfaces), and the main results have been summarized.

-Table 1 shows that the (101) surface has the highest population in the crystal morphology. However, according Figure 3, this surface has the highest density of the surface effects and the largest surface energy. I expect that in a process of the crystal growth surfaces with the lower energy are forming faster and, therefore, have larger population.

Answer: We agree with the Reviewer. However, we need to clarify that the surface energy values (Figure 3) are obtained from the calculations of the surface in vacuum. The ideal morphology (theoretical) is not the rod-like morphology, but the experimental morphology obtained along the synthesis is the elongated cubic-like (a parallelepiped). In our case, the resulted rod-like morphology is due to the stabilization/destabilization of (001), (010) and (101) surfaces during the process of dissolution/crystallization provoked by the microwave irradiation.

-In Fig. 4 what means CFU (not given in an abbreviation list)

Answer: As pointed out by the reviewer, CFU was inserted in the list of abbreviations.

-In references a proper formatting is needed (e.g. subscribes in chemical formula).

Answer: According to the reviewer, the references were formatted in the revised version of the manuscript.

In conclusion, I can recommend the paper to be published in the TCA journal after minor revision.

We are confident that considering the responses, this manuscript can be considered for publication in TCA.

We look forward to hearing from you.

On behalf of the authors,

Prof. Juan Andrés

Dr. Ilaria Ciofini & Prof. Carlo Adamo
Editors-in-Chief
Theoretical Chemistry Accounts (TCA)

Castellón, 20 May, 2020

Manuscript ID: TCAC-D-20-00072

Response to reviewers

We acknowledge the Reviewers for their help in improving our manuscript. As can be seen in the revised text, these comments, remarks and suggestions were considered during our revision. Detailed responses, point-by-point, to the reviewers are summarized below and the changes were made along the revised version of the manuscript and were highlighted in red color.

Reviewer #1: The surface-dependent reactivity with respect to the antibacterial and photocatalytic activity is discussed based on the α -Ag₂WO₄ NCs. The authors used their previous theoretical calculations on the α -Ag₂WO₄ to further discuss the surface-dependent properties of these materials including new experimental data. They used the antibacterial and photocatalytic activity to infer about the surface properties of NCs synthesized using different time exposure to microwaves.

The manuscript is well written providing an excellent discussion about the surface-dependent properties of α -Ag₂WO₄ and I recommend for publication after the authors address the concerns below.

1) The Table 1 and Figure 2 show a correlation between the exposure time to the microwaves and the polyhedron energy. It is well known that the morphologies can be changed with respect to the chemical potential and additives that stabilize one surface with respect to the other. However, the authors just explicit "The theoretical morphologies inserted in the polyhedron energy profile (fig 2) are calculated using the average experimental values of the width and length distribution of the crystals" (page 11, lines 33-35). In my point of view, this is ambiguous, since the proportion of (001) and (101) surfaces could change for the same value of width and length. In my point of

view, the values should also be coherent from the thermodynamics point of view. Larger exposure time of microwave should lead to more stable structure (smaller Epolyhedron). In my point of view, the authors should clarify this point.

Answer: The relative growth rate of each crystal surface along the synthesis process is linked to the appearance and/or disappearance of the exposed surfaces and depends on environmental conditions. These transformations are due to the geometric constraints imposed by the crystal structure and are associated with the relative values of the surface energy among the different of surfaces. In our methodology we calculated the surface energies values associating with the Wulff construction to obtain the complete set of available morphology that a given material can be displayed. We agree with the Reviewer's comment when he said that the values should also be coherent from the thermodynamics point of view. However, our focus here is justly demonstrate that through a simple methodology, that correlates the surface energy calculations with the Wulff construction, it is possible to obtain important information about the morphology of the samples, once that the properties of the materials are shape-dependent. Therefore, a note of caution is included in the revised version of the manuscript (see first paragraph of the section 2.1 Computational methods and model systems).

2) Please, include at the Electronic Supplementary Material information about the protocol used to perform the calculations and details of the slab models used (size, number of layers used, etc.) to avoid that the reader to go to the ref. [43] to get that information.

Answer: In the revised version, the protocol used to perform the calculations and details of the slab models used (size, number of layers used, etc.) was included in the Supporting Information (see section SI-2 Computational methods).

Reviewer #2: The manuscript deals with the combined theoretical and experimental study of silver tungstate semiconducting material (alpha polymorph, AWO). The work showed how theoretical methods based on density functional theory (DFT) calculations can help in the conducting and controlled material synthesis and design. Particularly, in the work the AWO microcrystals

were synthesized, and treated by microwave irradiation to show how such treatment can affect antibacterial and photocatalytic activity. Combining DFT calculations and knowledge about the morphology of microcrystals the authors explained activity of the dominant surfaces determining the overall shape of microcrystals. The experiments with *Staphylococcus aureus* and Rhodamine B showed that tuning microwave irradiation can lead to optimizing antibacterial activity and photocatalytic degradation. The work brings new knowledge about structural details and active sites of the AWO surfaces. Generally, the manuscript is well organized, the used methods are adequate and the achieved results accompanied with plausible discussion and interpretation. I have following comments and suggestions.

Microwave irradiation - control crystal growth - shape - morphology stays -rod-like hexagonal shape with - controlled but length less (fig. 1)

Answer: The time of microwave irradiation controls both the morphology and the size, as it is displayed in Figure 1

-Figure 2 shows the overall energy of AWO polyhedra with respect to time of irradiation - why is there a significant anomaly for the time 4 mins?

Answer: This anomaly can be associated to the fact that the sample obtained at $t = 4$ min, a destabilization of the (010) surface with concomitant increase of the $E_{polyhedron}$ value is sensed. In the revised version of the manuscript (see paragraph 1, page 11) this fact is now included.

-In Table 1 a contribution of surface energy of three surfaces to overall polyhedral energy is shown. While for the (001) and (101) surfaces the energy variation is in a reasonable range, for the (010) surface is a very large difference in values for 8 and 16 mins comparing to CP and 2/4 mins irradiation. Is this correct? If yes, why is there such big difference?

Answer: The modulation of the morphologies from experimental results is based on the width and length values from the distribution size of the particles. The width is governed by the (010) surface, while the length is derived from the surface energies values of the (001) surface. Therefore, the ratio between width and length values is the same between the (010) and (001) surfaces. To

maintain the rod-like morphology, the ratio between the values of the energy surface of both surfaces needs to be constant; therefore, the surface energy values of (101) surface are not modified. With the increase of the microwave irradiation time, the rod-like morphology suffers an elongation. This elongation is due to the increase of the (surface energy value for the (001) surface, and in order to compensate this increase, the surface energies of (010) need to be stabilized, i.e., its values decrease drastically (from 0.93 to 0.10 eV). However, in general, the percentage of contribution of (010) surface is almost equal in all morphologies (around 15%).

-In the manuscript no details are given about DFT method and parameters of used periodic slabs in calculations of surface energies. In this context, the manuscript refers to the previous work (ref. 43). Indeed, for the easier orientation of a potential reader, I recommend to add these details to the present manuscript as well. Also information about magnetic state of AWO slabs is missing.

Answer: As we write previously in the question 2 of the reviewer 1, in the revised version, the protocol used to perform the calculations and details of the slab models used (size, number of layers used, etc.) was included in the Supporting Information (see SI-2 Computational methods). With respect to magnetic behavior of AWO, this point is out of the main goal of present work. In future analysis, the corresponding spin densities of the exposed surfaces (at the morphologies), i.e. the magnetic state, will be considered.

-The authors explain the surface activity by a presence of electron-hole (e-h) pairs at surfaces as a consequence of defected sites (incomplete Ag/W coordination, deformed polyhedral units). How these defects are stable with respect to e.g. interaction with water molecules? Is there a study about that?

Answer: In our work, the presence of defect sites is associated to the incomplete Ag/W coordination, deformed polyhedral units. These defects provoke instability and are responsible of the generation of very reactive species with radical behavior, i.e. presence of oxygen vacancies, unpaired electrons, etc. Therefore, these defects are the active sites where the reaction with water molecules, for example, takes place. In the present

experimental/theoretical work this innovative mechanism is proposed (see last paragraph of section 3.2 Antibacterial and photocatalytic activity and conclusions section).

-For better understanding of reactivity of surface sites electronic structure (density of states and band gaps) of different surface models could be useful. Did the authors performed an analysis of the electronic structure of the surface slab models?

Answer: The band gaps of different surface models were previously reported. The density of states was analyzed for the set of surfaces presented in the morphologies. The undercoordinated clusters of Ag and W atoms on the top of each surface were analyzed in the manuscript. In the revised Supporting Information (see section SI-3.4 Theoretical analysis of the surfaces), and the main results have been summarized.

-Table 1 shows that the (101) surface has the highest population in the crystal morphology. However, according Figure 3, this surface has the highest density of the surface effects and the largest surface energy. I expect that in a process of the crystal growth surfaces with the lower energy are forming faster and, therefore, have larger population.

Answer: We agree with the Reviewer. However, we need to clarify that the surface energy values (Figure 3) are obtained from the calculations of the surface in *vacuum*. The ideal morphology (theoretical) is not the rod-like morphology, but the experimental morphology obtained along the synthesis is the elongated cubic-like (a parallelepiped). In our case, the resulted rod-like morphology is due to the stabilization/destabilization of (001), (010) and (101) surfaces during the process of dissolution/crystallization provoked by the microwave irradiation.

-In Fig. 4 what means CFU (not given in an abbreviation list)

Answer: As pointed out by the reviewer, CFU was inserted in the list of abbreviations.

-In references a proper formatting is needed (e.g. subscribes in chemical formula).

Answer: According to the reviewer, the references were formatted in the revised version of the manuscript.

In conclusion, I can recommend the paper to be published in the TCA journal after minor revision.

We are confident that considering the responses, this manuscript can be considered for publication in TCA.

We look forward to hearing from you.

On behalf of the authors,

Prof. Juan Andrés

[Click here to view linked References](#)

Surface-dependent properties of α -Ag₂WO₄: a joint experimental and theoretical investigation

Leticia O. Laier¹, Marcelo Assis², Camila C. Foggí², Amanda F. Gouveia³,
Carlos E. Vergani⁴, Luís C. L. Santana⁴, Laécio S. Cavalcante³, Juan Andrés^{5*},
and Elson Longo²

¹CDMF, LIEC, Instituto de Química, Universidade Estadual Paulista, P.O. Box 355, 14800-900, Araraquara-SP, Brazil.

²CDMF, LIEC, Chemistry Department of the Federal University of São Carlos, P.O. Box 676, 13565-905 São Carlos-SP, Brazil.

³Departamento de Química, Universidade Estadual do Piauí, P.O. Box 381, CEP 64002-150, Teresina-PI, Brazil

⁴São Paulo State University (UNESP), P.O. Box 1680, 14801903, Araraquara-SP, Brazil.

⁵Department of Analytical and Physical Chemistry, Universitat Jaume I (UJI), 12071 Castelló, Spain.

Corresponding author: andres@qfa.uji.es

Abstract

α -Ag₂WO₄ has attracted much attention in recent years due to its unique crystal and electronic structures, which are suitable for a wide range of applications. This work presents a more realistic study, based on first-principles calculations and experimental results, of the potential of α -Ag₂WO₄ for antibacterial and photocatalytic activity. α -Ag₂WO₄ material has been successfully synthesized by a coprecipitation method and subjected to microwave irradiation for different times. The as-synthesized microcrystals were structurally characterized by X-ray diffraction, while the morphological aspects were investigated by field emission scanning electron microscopy. The experimental studies and theoretical simulations of α -Ag₂WO₄, based on density functional theory calculations, have highlighted several key parameters (surface-dependent) that determine the antibacterial (against *Staphylococcus aureus*) and photocatalytic activity (for the degradation of Rhodamine B), and provided some general principles for materials design. We believe that our results offer new insights regarding the local coordination of superficial Ag and W cations (i.e. clusters) on each exposed surface of the corresponding morphology, that dictate the antibacterial and photocatalytic activities of α -Ag₂WO₄, a field that has so far remained unexplored.

Keywords: α -Ag₂WO₄, morphology, antibacterial and photocatalytic activity.

1 Introduction

This manuscript is dedicated to Professor Dr. Fernando R. Ornellas at the 70th birthday. He is a pioneer with notable achievement in the theoretical and computational chemistry in Brazil. He has an outstanding international reputation as an educator and researcher.

The semiconductor silver tungstate (α -Ag₂WO₄ - AWO) is an important multifunctional material that has interesting physical and chemical properties with a wide range of applications. Thus, it could be used as an effective photocatalyst for the degradation of dyes under visible light irradiation [1–10], a bifunctional catalyst [11], gas sensing, tumor identification and uptake [12], antimicrobial activity against *Escherichia coli* and *Staphylococcus aureus* (*S. aureus*), and its antifungal activity against *Candida albicans*, amongst others [1, 2, 18–25, 3–5, 13–17]. Its superior performances can be associated with its strong photo-sensitizing ability and particular structure, which is composed of [WO₆] and [AgO_y] ($y = 2, 4, 6$ and 7) clusters [26–28], as the building blocks of the material, and its electronic properties [3, 29, 30], which can be associated with structural order-disorder effects on the crystal lattice [3].

Different methods of synthesis are employed to obtain AWO crystals with well-defined homogeneous size and morphology[6]. Among these methods, the solid state reaction [21], sol-gel and conventional hydrothermal [31–34] methods are routinely used. Most of these methods require an extended amount of time for the synthesis of microcrystals as well as extreme conditions [32]. Microwave irradiation has been widely applied for the synthesis of inorganic materials at relatively lower temperatures and in a shorter time (e.g. in minutes), compared to conventional heating [35–37]. The advantages of using

1 microwaves include the low cost, ease and speed of preparing crystalline
2 samples, and especially the production of materials with higher phase purity
3 and narrow particle size distribution [38–42]. An attractive alternative, although as
4 yet underexplored, strategy to gain control over these properties is provided by
5 regulating the microwave irradiation while keeping all the other parameters
6 constant.
7
8
9
10
11
12
13

14 The active sites of a given material can be difficult to identify and
15 understand and, hence, the introduction of active sites, for example in the
16 surfaces of catalysts, in order to tailor their function is challenging. Regardless
17 of the possible advances in synthesis routes, there is a clear need for
18 systematic ways to search for the potential material design space to narrow
19 down the focus on the exposed surfaces of materials that are expected to be
20 high-performing. In this context, the exposed surfaces appearing in the
21 morphology profoundly affect the properties and are essential to their
22 performance, as they are often considered to be active sites for their reactivity.
23
24 A photocatalytic process initiates when the catalyst absorbs a photon of greater
25 energy than its energy band gap, thereby generating electron-hole pairs, (e^-h^*).
26
27 Some of them recombine and release their energy, while others are used to
28 participate in oxidation-reduction reactions on the surface of the catalyst, thus
29 producing reactive oxygen species (ROS). In particular, the surface energy not
30 only determines the surface structure and stability of the exposed surfaces but
31 also reflects the catalytic activity [21]. Density functional theory (DFT)
32 calculations [43] on extended surfaces have revealed the structures and the
33 energy of six low-index stoichiometric surfaces: (100), (010), (001), (110), (101)
34
35
36
37
38
39
40
41
42
43
44
45
46
47
48
49
50
51
52
53
54
55
56
57
58
59
60
61
62
63
64
65

1
2
3
4
5
6
7
8
9
10
11
12
13
14
15
16
17
18
19
20
21
22
23
24
25
26
27
28
29
30
31
32
33
34
35
36
37
38
39
40
41
42
43
44
45
46
47
48
49
50
51
52
53
54
55
56
57
58
59
60
61
62
63
64
65

and (011) of AWO. However, the role of the exposed surfaces and morphology in the antibacterial and photocatalytic activity has still not been revealed.

Inspired by the above considerations, in this work we report the synthesis of AWO by the coprecipitation (CP) method, with the as-synthesized samples being subjected to microwave irradiation for different times. Therefore, the structure was confirmed using X-ray diffraction (XRD) with Rietveld refinement, micro-Raman (MR) and Fourier transform infrared (FT-IR) spectroscopies. Their optical properties were investigated by ultraviolet-visible (UV-Vis) diffuse reflectance spectroscopy and photoluminescence (PL) measurements at room temperature. Field emission-scanning electron microscopy (FE-SEM) images were employed to monitor the evolution of the shape, size and growth process of the crystals as the time of microwave irradiation increases. In order to complement these experimental results and aid the interpretation of the experimental results, first-principles calculations within the framework of DFT were performed. The performances of the as-synthesized AWO samples with antibacterial (against *S. aureus*) and photocatalytic activity (for the degradation of Rhodamine B, RhB) will be demonstrated. Finally, a surface-dependent antibacterial and photocatalytic activity relationship was established, which may serve as a guideline for designing high performance AWO based materials. The goal of this work is three-fold: (i) to determine the energy profiles associated with the morphology transformation processes at different microwave irradiation times, (ii) to demonstrate, for first time, the antibacterial activity of AWO, obtained by the above procedure, towards *S. aureus*, and (iii) to find a correlation between the morphology and the antibacterial and photocatalytic activity.

1 This paper contains three more sections. The next is the experimental
2 section, which describes the techniques for the preparation and characterization
3 of the samples, computational methods and model systems and the
4 antibacterial and photocatalytic measurements. In section three, the results are
5 presented and discussed. The main conclusions are summarized in the fourth
6 section.
7
8
9
10
11
12
13
14
15
16

17 **2 Experimental Methods**

18
19 Samples of AWO were synthesized by the coprecipitation method at 90°C,
20 in an aqueous medium as described by our research group [29]. After
21 precipitation, the suspensions were transferred to a Teflon® autoclave, sealed
22 and placed in a microwave-assisted hydrothermal system (2.45 GHz, maximum
23 power of 800 W). The reaction mixtures were submitted to microwave irradiation
24 at 140°C for 2, 4, 8, and 16 min. The products were washed several times with
25 deionized water and dried at 65°C for 12h. The characterization techniques
26 have been presented in the Supporting Information (SI).
27
28
29
30
31
32
33
34
35
36
37
38
39
40

41 **2.1 Computational methods and model systems**

42
43 The surface energy values (E_{surf}) of the six low-index crystal surfaces,
44 (100), (010), (001), (110), (101) and (011) of AWO have been obtained from our
45 previous calculations[43] and details can be found on the SI, showing that it is
46 possible not only to determine the equilibrium shape and ideal morphology,
47 using the Wulff construction, but also to find a map of available morphologies
48 for AWO. The procedure to obtain the complete set of morphologies, based on
49 the Wulff construction and the values of E_{surf} , has been previously presented
50
51
52
53
54
55
56
57
58
59
60
61
62
63
64
65

1
2
3
4
5
6
7
8
9
10
11
12
13
14
15
16
17
18
19
20
21
22
23
24
25
26
27
28
29
30
31
32
33
34
35
36
37
38
39
40
41
42
43
44
45
46
47
48
49
50
51
52
53
54
55
56
57
58
59
60
61
62
63
64
65

by our research group [43] and was successfully used to obtain the morphology of materials, including PbMoO_4 , $\alpha\text{-Ag}_2\text{MoO}_4$, BaMoO_4 , BaWO_4 , CaWO_4 , Ag_3PO_4 , Ag_2CrO_4 and LaVO_4 [44–51]. At this point, it is pertinent to note that this methodology is based on the classic Wulff construction of clean surfaces to obtain the complete set of available morphology of a given material.

The energy profiles linking the ideal and given morphologies are found by changing the relative E_{surf} values of each surface [15, 43]. In this method, different morphologies are connected by energy profiles according to their polyhedron energy ($E_{polyhedron}$) values. The $E_{polyhedron}$ is defined as:

$$E_{polyhedron} = \sum_i C_i \times E_{surf}^i \quad (1)$$

where C_i is the percentage contribution of the surface area to the total surface area of the polyhedron, $C_i = A^i / A^{polyhedron}$, and E_{surf}^i is the E_{surf} of the corresponding surface [21].

In addition, the broken bonding density (D_b), defined as the number of broken bonds per unit cell area when a surface is created, can be calculated by using equation 2 [52, 53]:

$$D_b = N_b / A \quad (2)$$

where N_b is the number of broken bonds per unit cell area on a specific surface and A is the area unit of the surface. From the values of D_b it is possible to predict the order of surface stability, i.e. higher values of D_b are obtained when larger numbers of defects are present in the surface [54].

2.2 Antibacterial and photocatalytic measurements

1 The antibacterial activity of the AWO samples was tested using the broth
2 microdilution method against *S. aureus* obtained from the American Type
3 Culture Collection (ATCC 25923) as previously described [3, 30]. The standards
4 described by the Clinical and Laboratory Standards Institute (CLSI) [55] were
5 used, with modifications [30, 56].
6
7
8
9
10

11 The photocatalysis of the AWO samples with respect to the degradation of
12 RhB (95%, Mallinckrodt) in aqueous solution was performed as described
13 previously, under UV light [57]. Briefly, the suspensions containing the
14 individually place synthesized samples (50 mg) and RhB solution (1.63×10^{-5}
15 mol.L⁻¹ / 50 mL) were ultrasonicated before illumination for 5 min at a frequency
16 of 42 kHz, and stored in the dark for 5 min to promote the adsorptive processes.
17 The suspensions were then placed (one at a time) in a photo-reactor and
18 illuminated using six UV lamps (TUV Phillips, 15 W and intensity at 254 nm). At
19 30 min intervals aliquots were removed, centrifuged and analysed by UV-vis
20 spectroscopy using a double-beam spectrophotometer with a double
21 monochromator and a photomultiplier tube detector (JASCO V-660, USA).
22
23
24
25
26
27
28
29
30
31
32
33
34
35
36
37
38
39
40

41 **3 Results and Discussion**

42 Generally, the reactivity of a material is mainly determined by its size,
43 morphology, composition and surface structure. In particular, its morphology
44 has a direct influence on its number of active sites. Therefore, the focus is on
45 controlling the morphology in order to achieve higher antibacterial and
46 photocatalysis performance, which is still very challenging because of the high
47 experimental costs, limited time resolution and short observation times, etc. The
48 combination of experimental observation and theoretical modelling is an
49
50
51
52
53
54
55
56
57
58
59
60
61
62
63
64
65

1 effective way to provide insight into the reshaping phenomenon and to go
2 beyond the technical limits. To this end, a computational investigation was
3
4 conducted to find the nature of the clusters on each exposed surface, i.e. local
5 coordinations of both Ag and W cations, and then to determine the relationship
6
7 among the nature of these clusters in terms of the morphology and the
8
9 antibacterial and photocatalytic activity.
10
11
12
13
14
15

16 **3.1 FE-SEM images**

17
18
19 Different parameters (temperature, solvent, pH, pressure, agitation, etc.)
20 control the morphology and size of the AWO samples that are obtained [15, 16,
21
22 26]. **Figure 1** shows FE-SEM images of the samples. The morphology
23
24 observed for all the samples was rod-like with a hexagonal shape, as shown in
25
26 the inset of the images, formed by the combination of only three surfaces: the
27
28 (010), (001) and (101) surfaces.
29
30
31
32
33
34
35
36
37
38
39
40
41
42
43
44
45
46
47
48
49
50
51
52
53
54
55
56
57
58
59
60
61
62
63
64
65

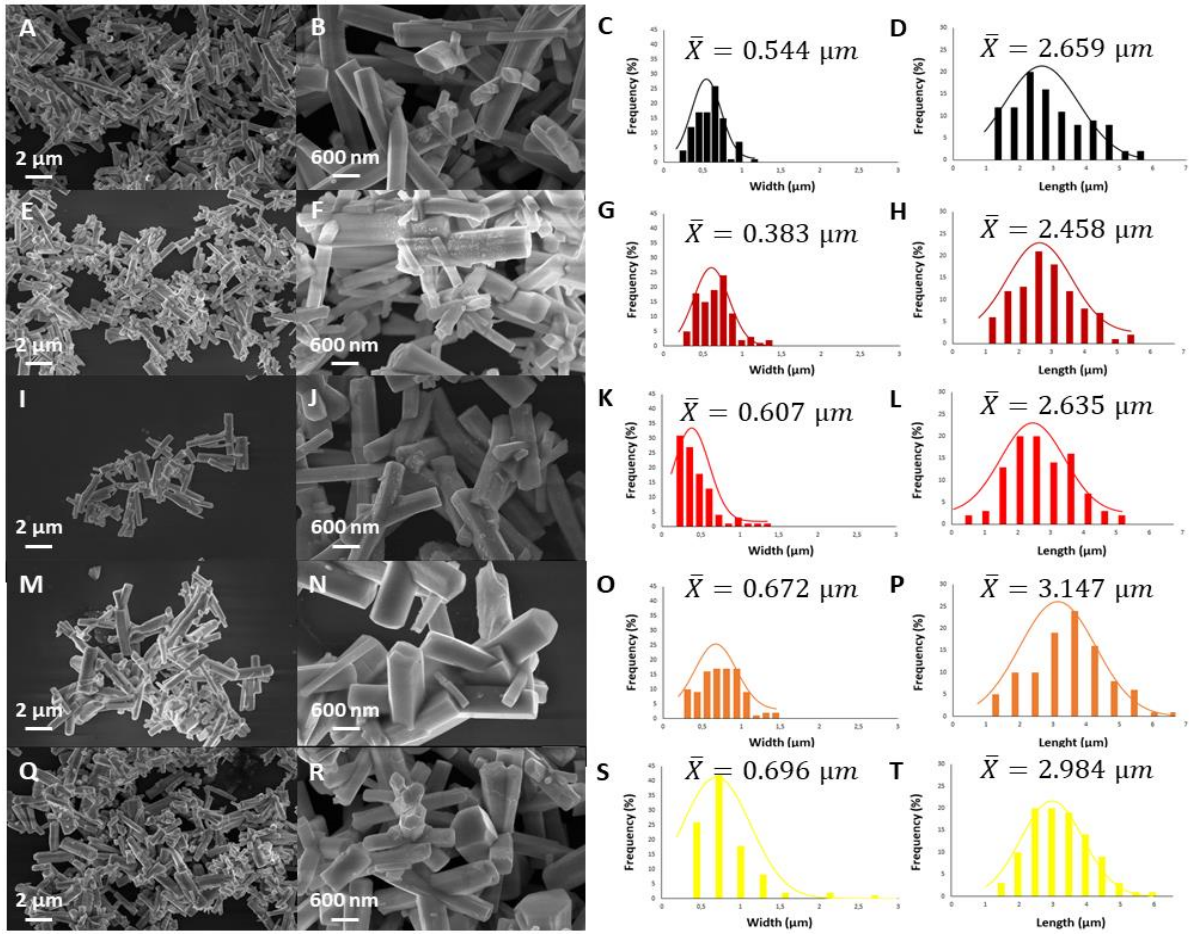


Figure 1. FE-SEM images of AWO microcrystals synthesized by the CP method followed by microwave irradiation and average width and length distribution of the crystals: (A-D) CP, (E-H) 2 min, (I-L) 4 min, (M-P) 8 min, (Q-T) 16 min.

The samples obtained by the CP without microwave irradiation have a mean width and length of 0.544 and 2.659 μm , respectively. When the material is subjected to irradiation for 2 min, these values are reduced to 0.383 and 2.457 μm , respectively. As the time of microwave irradiation increases, the mean width and length increase gradually, leading to values of 0.383 and 2.457 μm , 0.609 and 2.635 μm , 0.672 and 3.147 μm , and 0.696 and 2.983 μm for the samples synthesized at 4, 8 and 16 min, respectively. These variations modify the structure and electronic properties of the exposed surfaces in the corresponding morphology, and then enhancing/diminishing the separation

processes of the $(e'-h^*)$ responsible for the antibacterial and photocatalytic activity.

In order to correlate the effect of the change in morphology observed in the FE-SEM images, we take into account the (100), (010), (001), (110), (101) and (011) surfaces of AWO. From the values of the E_{surf} and using the Wulff construction, the complete map of available morphologies is obtained. From here, the $E_{polyhedron}$ values of each morphology are calculated to be able to draw an energy profile, as displayed in **Figure 2**.

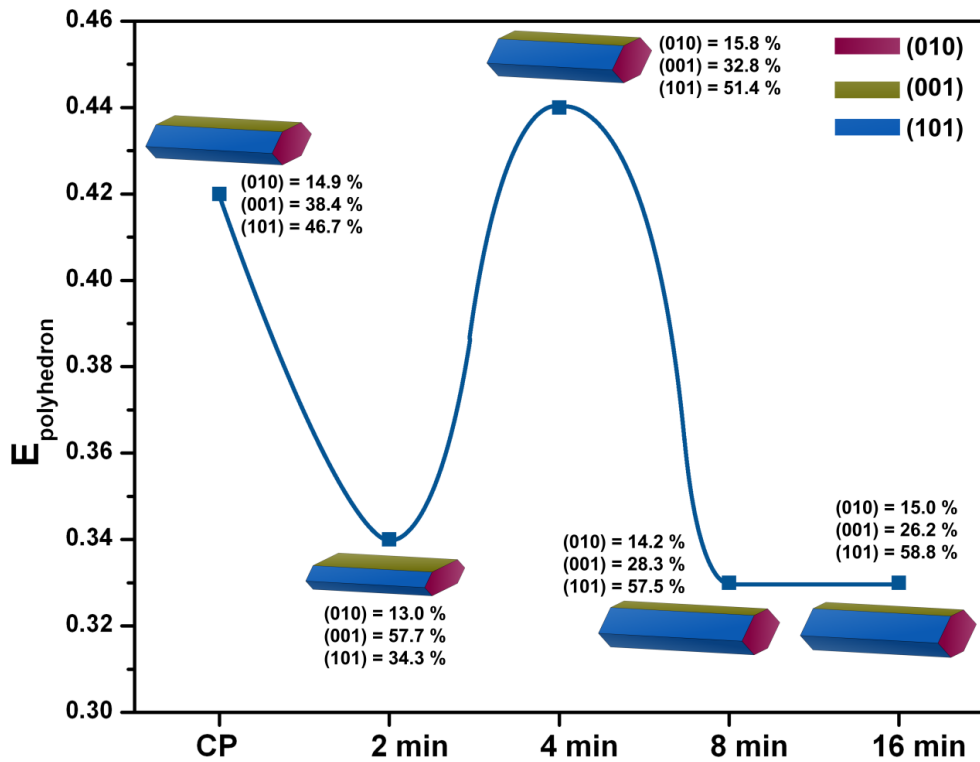


Figure 2. Polyhedron energy profiles and the morphologies for the AWO samples synthesized by the CP method followed by microwave irradiation for different times.

The theoretical morphologies inserted in the polyhedron energy profile (**Figure 2**) are calculated using the average experimental values of the width

and length distribution of the crystals. These results show that microwaves decrease the size of the AWO samples due to simultaneous dissolution and crystallization processes [33], but not necessary results in a morphology with low value of $E_{polyhedron}$. This fact is observed in $t = 4$ min, when the value of $E_{polyhedron}$ corresponds to a maximum in the energy profile, due to the destabilization of the (010) surface.

By increasing the exposure time, a preferential growth process favours the appearance of the (001) surface, while the (010) surface is destabilized, as confirmed by the values of the surface energies in **Table 1**.

Table 1. Surface energy for each surface (E_{surf}^i , $J.m^{-2}$), percentage of contribution of the surface area by the total area (C_i , %) and polyhedron energy ($E_{polyhedron}$, $J.m^{-2}$).

Morphology	$E_{surf}^i (C_i)$			$E_{polyhedron}$
	(010)	(001)	(101)	
CP	0.93 (14.9)	0.23 (38.4)	0.40 (46.7)	0.42
2 min	0.86 (13.0)	0.16 (57.7)	0.40 (34.3)	0.34
4 min	0.93 (15.8)	0.26 (32.8)	0.40 (51.4)	0.44
8 min	0.11 (14.2)	0.29 (28.3)	0.40 (57.5)	0.33
16 min	0.10 (15.0)	0.30 (26.2)	0.40 (58.8)	0.33

A detailed analysis of the results from **Table 1** and **Figure 2** shows that the microwave irradiation first affects the (001) surface ($t = 2$ min), stabilizing it and yielding a morphology with low polyhedron energy. As the time in the microwave irradiation increases ($t = 4$ min), there is an increase in the presence of the (010) surface. This pathway results in a high $E_{polyhedron}$ value, via a maximum (see **Figure 2**). For the next two samples ($t = 8$ and 16 min), a

1 decrease and an increase in the surface energy of the (010) and (001) surfaces
2 occurs, respectively. The joint stabilization of the (010) surface and the
3 destabilization of the (001) surface are responsible for the final morphology,
4
5 which corresponds to the minimum in **Figure 2**.
6
7

8
9 An atomic level description of the top of each exposed surface reveals the
10 presence of defects, in the form of undercoordinated clusters, i.e. local
11 coordinations of both Ag and W cations with the presence of oxygen vacancies
12 and complete distorted clusters. Using the Kröger-Vink notation [58], the oxygen
13 vacancy can be written as V_o^x and presents a neutral charge (x) [59], whereas
14 the distorted clusters can be represented by the subindex (d). The distorted
15 clusters of AWO are the building blocks of the lattice, composed of $[AgO_y]_d$ ($y =$
16 2, 4, 6 and 7) and $[WO_6]_d$. Using this representation, it is possible to analyse
17 the kind of undercoordinated clusters with the presence of both V_o^x and
18 complete clusters involved in the rod-like hexagonal morphology, and also the
19 broken bonds density (D_b) for each surface [60]. **Figure 3** displays the three
20 surfaces that appear in the AWO morphology, i.e. the (010), (001) and (101)
21 surfaces, where the surface energy values are from the slab calculations [43]
22 and also the calculated value of D_b for each surface. The electronic properties
23 of the AWO bulk and surfaces were summarized in the SI (see Section SI-3.4).
24
25 The (010) surface is formed by $[AgO_5 \cdot 2V_o^x]$ undercoordinated clusters and by
26 $[AgO_4]_d$ and $[WO_6]_d$ distorted clusters. The (001) surface is composed of the
27 $[AgO_4 \cdot 3V_o^x]$, $[AgO_4 \cdot 2V_o^x]$, $[AgO_5 \cdot 2V_o^x]$ undercoordinated clusters and of the
28 $[WO_6]_d$ distorted clusters in the first layer and the $[WO_5 \cdot V_o^x]$ clusters in the
29 second layer. On the other hand, the (101) surface is formed by the $[WO_5 \cdot V_o^x]$
30
31
32
33
34
35
36
37
38
39
40
41
42
43
44
45
46
47
48
49
50
51
52
53
54
55
56
57
58
59
60
61
62
63
64
65

cluster in the first layer, the $[AgO_4 \cdot 3V_o^x]$ and $[AgO_5 \cdot 2V_o^x]$ clusters in the second layer and the $[WO_5 \cdot V_o^x]$ and $[WO_6]_d$ clusters in the third layer.

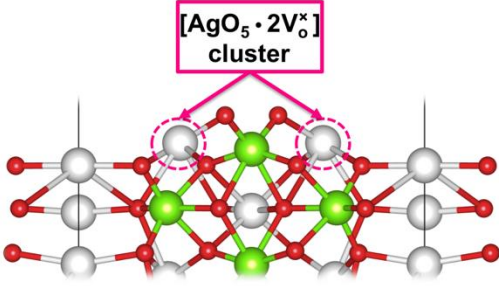
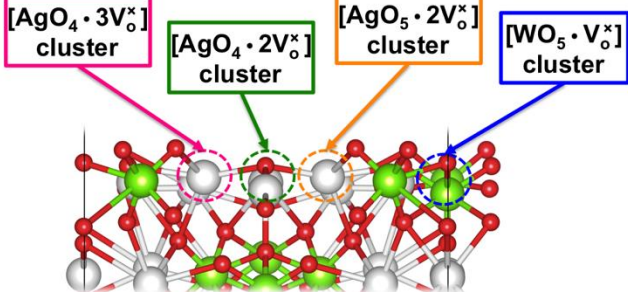
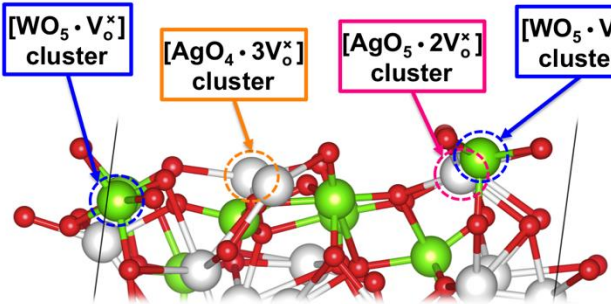
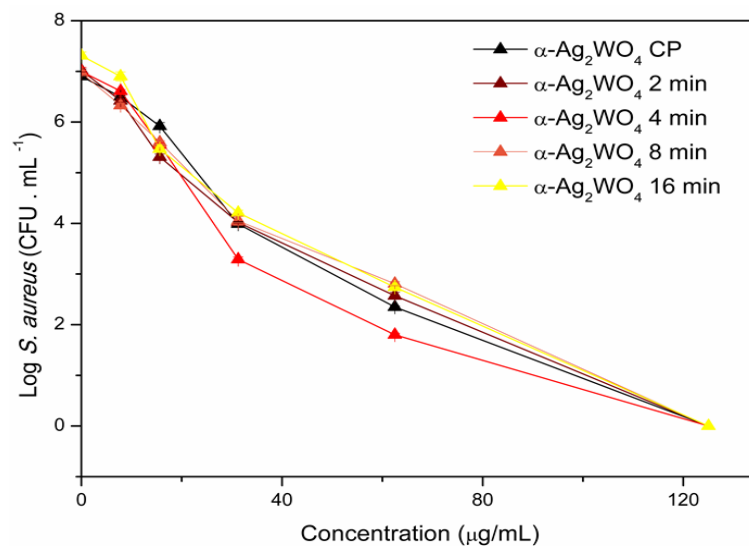
(010) surface	
Model	Broken bond density (D_b)
	$N_b = 4$ $A = 0.601 \text{ nm}^2$ $D_b = 6.66 \text{ nm}^{-2}$
	Surface Energy (E_{surf})
	$E_{\text{surf}} = 0.20 \text{ J}\cdot\text{m}^{-2}$
(001) surface	
Model	Broken bond density (D_b)
	$N_b = 13$ $A = 1.325 \text{ nm}^2$ $D_b = 9.81 \text{ nm}^{-2}$
	Surface Energy (E_{surf})
	$E_{\text{surf}} = 0.53 \text{ J}\cdot\text{m}^{-2}$
(101) surface	
Model	Broken bond density (D_b)
	$N_b = 16$ $A = 1.492 \text{ nm}^2$ $D_b = 10.72 \text{ nm}^{-2}$
	Surface Energy (E_{surf})
	$E_{\text{surf}} = 0.68 \text{ J}\cdot\text{m}^{-2}$

Figure 3. Surface model with the undercoordinated clusters on the top of each surface, surface broken bonds density (D_b), and, surface energy value (E_{surf} , $\text{J}\cdot\text{m}^{-2}$) reported by Ref [43].

1 The D_b value provides a direct relationship between the surface energy
2 value and the number of broken bonds. In this way, the most stable (010)
3 surface shows low values of E_{surf} and D_b , which means that the (010) surface
4 shows low values of E_{surf} and D_b , which means that the (010) surface
5 has a small number of defects in the surface. Conversely, the (101) surface has
6 the highest values of E_{surf} and D_b , and is the most active site in terms of their
7 reactivity [21].
8
9
10
11
12
13
14
15
16
17

18 3.2 Antibacterial and photocatalytic activity

19 The antibacterial activity for the AWO samples was tested against *S. aureus*
20 and the results are shown in **Figure 4**. From an analysis of these results it is
21 possible to conclude that all the materials presented antibacterial activity
22 against *S. aureus*. For each of the synthesized samples, namely α - Ag_2WO_4
23 obtained by the CP method, and after microwave irradiation for 2, 4, 8 and 16
24 min, the MBCs were well matched to each other (125 $\mu\text{g}/\text{mL}$), as shown in
25
26
27
28
29
30
31
32
33
34 **Figure 4**.
35
36
37
38
39



1
2
3
4
5
6
7
8
9
10
11
12
13
14
15
16
17
18
19
20
21
22
23
24
25
26
27
28
29
30
31
32
33
34
35
36
37
38
39
40
41
42
43
44
45
46
47
48
49
50
51
52
53
54
55
56
57
58
59
60
61
62
63
64
65

Figure 4. Summary of log₁₀ colony forming unit (CFU.mL⁻¹) values of *S. aureus* obtained for the subinhibitory concentrations of the microcrystals synthesized by CP method followed by microwave irradiation.

Although the MBCs were coincident between the samples, it can be observed that at sub-inhibitory concentrations (sub-MIC), the 4 min AWO material had a smaller number of colony forming units (CFU) per mL than the other materials. This material presents a morphology with the highest $E_{polyhedron}$ value, a maximum along the energy profile, as shown by the theoretical results presented in **Figure 2**. This result can be associated to the presence of (010), (001) and (101), as exposed surfaces of the morphology, as shown in **Table 1**.

Several antimicrobial mechanisms of action have been suggested for AWO [3, 5, 25, 30, 61, 62]. For micrometre-sized materials, the most accepted mechanism is microbial elimination by oxidative processes. Electron excitation/recombination mechanisms in the internal structure of AWO would be responsible for the release of ROS, specifically O_2H^* [5], which inactivate the microorganisms [3], besides being essential in the photocatalytic process, and also play a role in the elimination of microorganisms. The sum of all these effects causes the death of the bacteria and can involve the following step: the contact between the bacterial cell and the exposed surfaces of AWO can enhance changes in the microenvironment within the area of contact between the microorganism and the particle. The ROS thus formed exhibit high oxidative potential to react with the carbon chains present in the bacterial wall, resulting in the breakdown of the chains of the lipid compounds, proteins, etc [3, 13, 25, 63]. Hence, it is hypothesized that the increased ROS may further trigger

1 catalyzing oxidation reactions [64], and the exposed surfaces of AWO produce
2 a stronger interaction with the bacterial cells to react with the carbonic chains,
3
4 and cause destabilization of the phospholipid bilayer of the cell and degradation
5
6 of cytosolic proteins (i.e. DNA). This triggers cell death and the generation of
7
8 ROS, which leads to increased oxidative stress and cell instability [65, 66].
9

10
11
12 Very recently, Nobre *et al.* [25] have demonstrated that AWO microcrystals
13
14 were effective in the inhibition of bacterial (methicillin-resistant *Staphylococcus*
15
16 *aureus*, MRSA, and enterohaemorrhagic *Escherichia coli*, EHEC) and fungi
17
18 (*Candida albicans*, *C. abicans*, and *Trichophyton rubrum*, *T. rubrum*) cell
19
20 growth. In particular, these authors show the high antibacterial and antifungal
21
22 activity of rod-like AWO synthesized by sonochemistry (SC) and the
23
24 conventional hydrothermal-assisted ultrasound method (SC+HC), at different
25
26 times (1, 6 and 12h – SC+HC-1h, SC+HC-6h and SC+HC-12h, respectively).
27
28 The MIC values found for MRSA were 2x lower for SC + HC-6h and SC + HC-
29
30 12h samples compared to the others, in the microdilution test followed by
31
32 plating on agar. Inactivation of MRSA required a concentration of 250 µg/mL.
33
34 Although there are differences between the bacterial strains used in the two
35
36 studies, in this work the same test was performed with methicillin susceptible *S.*
37
38 *aureus* for all samples, and the corresponding MIC was 125 µg/mL.
39
40
41
42
43
44
45

46 The photocatalytic performance of AWO samples was tested via
47
48 degradation of RhB under UV light. The photodegradation of RhB by AWO was
49
50 analysed using the exponential decay of the curve C/C_0 . As shown in **Figure 5**,
51
52 all compounds can completely degrade RhB after 210 min under UV-Vis light,
53
54 as demonstrated by the decay of the localized absorption band at 554 nm. This
55
56 decay occurs because the xanthene ring (RhB conjugated chromophore)
57
58
59
60
61
62
63
64
65

undergoes a gradual di-ethylation in the functional groups N,N'-diethylammonium, causing a hypochromic displacement in absorption[67].

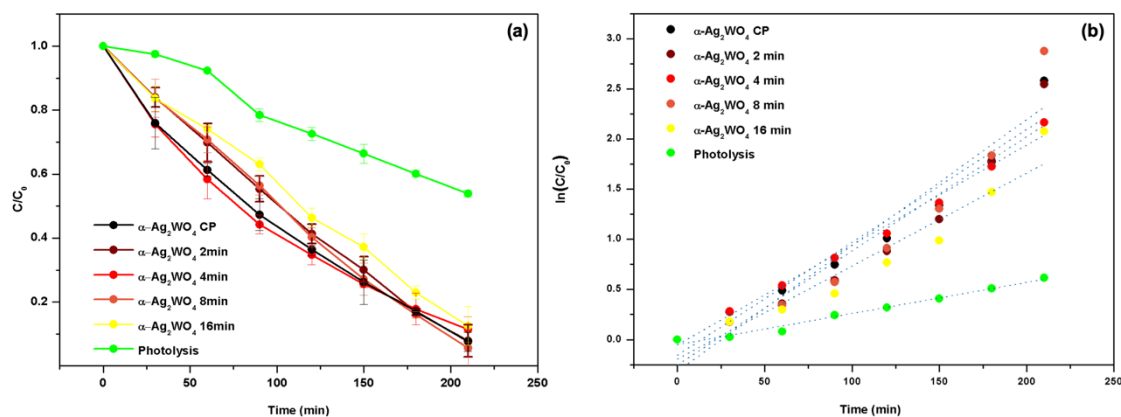


Figure 5. (a) Photocatalytic degradation of RhB composites of AWO at different times spectra after 210 min of UV-VIS irradiation and (b) first-order kinetic plots.

To quantitatively understand the reaction kinetics for the photodegradation of RhB by AWO, the pseudo-first order model expressed in equation 3 was applied to obtain the velocity constants (k):

$$\ln\left(\frac{C}{C_0}\right) = kt \quad (3)$$

where C_0 is the initial concentration ($t = 0$ min) of the dye solution, C is the concentration of the dye with different times of exposure to UV light, t is the time and k is the pseudo-first order constant. According to equation 3, a line with slope k (Figure 5b) is obtained from this graph.

Table 2 shows the results for the specific surface area (S_{BET}) of each sample and their respective speed constants k ($k_{absolute}$ and $k_{normalized}$).

Table 2. S_{BET} ($m^2.g^{-1}$) of each sample and their respective speed constants k , $k_{absolute}$ (s^{-1}) and $k_{normalized}$ ($s^{-1}.m^{-2}.g$).

Sample	S_{BET}	$k_{absolute}$	$k_{normalized}$
α -Ag ₂ WO ₄ - CP	2.677	1.12×10^{-2}	4.18×10^{-3}
α -Ag ₂ WO ₄ - 2 min	1.459	1.14×10^{-2}	7.81×10^{-3}
α -Ag ₂ WO ₄ - 4 min	1.810	9.96×10^{-3}	5.50×10^{-3}
α -Ag ₂ WO ₄ - 8 min	2.021	1.25×10^{-2}	6.18×10^{-3}
α -Ag ₂ WO ₄ - 16 min	2.169	9.27×10^{-3}	4.27×10^{-3}
Photolysis	–	3.10×10^{-3}	–

In this case, as the particle size decreases, the surface area also decreases. Small variations are seen in the constant $k_{absolute}$. As the as-synthesized samples become more organized by the effect of the microwave irradiation, there is a decrease in the constant $k_{absolute}$, in relation to the material obtained by the CP method. This occurs because, when the material has a high degree of disorder, a decrease in the $e'-h^*$ recombination process occurs, increasing the photocatalytic activity. When normalizing $k_{absolute}$ by S_{BET} , as the size of the surface area increases, the value of the $k_{normalized}$ decreases. An increase in the specific surface enhances the photocatalytic activity at specific AWO sites, but this does not mean that the specific surface area is directly related to photocatalytic efficiency, as the photocatalytic processes of AWO occur as a result of the greater exposure of the (101) surface[21]. In previous work[57], AWO was synthesized by means of the microwave-assisted method at different temperatures and applied to the photodegradation of RhB. The sample

1 prepared at 140°C presented a $k_{\text{normalized}}$ value of 8.45×10^{-3} , very similar to the
2 values reported here.
3

4 The photodegradation activities using the AWO materials were evaluated
5 with respect to the RhB degradation process. Both OH^* and O_2' radicals are the
6 oxidizing species[16, 41, 59]. The standard mechanism proposed by Zhang *et*
7 *al.*[68] for the photocatalytic reaction involved the formation of $e'-h^*$ pairs,
8 followed by interaction with O_2 and H_2O , respectively. Among the samples, the
9 AWO obtained after 4 min of microwave irradiation presented the best
10 antibacterial and photocatalytic activity. According to the theoretical
11 calculations, the morphology present by these samples has the highest
12 $E_{\text{polyhedron}}$ value, which is associated to the presence of (010), (001) and (101)
13 surfaces.
14
15
16
17
18
19
20
21
22
23
24
25
26
27

28 The main factor responsible for both the photocatalytic and the antibacterial
29 activity of AWO is a low recombination rate between photogenerated $e'-h^*$ pairs
30 on the surface of the AWO. Thus, it is necessary to go beyond the analysis of
31 the $[WO_6]$ and $[AgO_y]$ ($y = 2, 4, 6$ and 7) clusters, which are directly connected
32 to the structural and electronic order/disorder in the bulk material. Therefore, the
33 investigation was focused on the analysis of the structural and electronic
34 characteristics of both undercoordinated and distorted clusters appearing in the
35 exposed surfaces, (010), (001) and (101), in the morphology. This method is
36 helpful to clarify the nature of $e'-h^*$ localization in the constituent clusters at the
37 surfaces, providing an atomic level point of view of the fundamental mechanism
38 associated with electron excitation and localization, which are responsible for
39 many phenomena, such as antibacterial and photocatalysis activity.
40
41
42
43
44
45
46
47
48
49
50
51
52
53
54
55
56
57
58
59
60
61
62
63
64
65

1
2
3
4
5
6
7
8
9
10
11
12
13
14
15
16
17
18
19
20
21
22
23
24
25
26
27
28
29
30
31
32
33
34
35
36
37
38
39
40
41
42
43
44
45
46
47
48
49
50
51
52
53
54
55
56
57
58
59
60
61
62
63
64
65

The initial step in the photocatalytic activity involves the formation of the $e'-h^*$ pair and, therefore, the anisotropy of the electronic properties of these surfaces will promote the separation of the light-excited $e'-h^*$ pair. In the (010) surface, there is an accumulation of e' in the complete $[AgO_4]_d$ and distorted $[WO_6]_d$ clusters and there is e' depletion, positive charge accumulation, in the $[AgO_5 \cdot 2V_o^x]$ undercoordinated cluster, creating a potential difference, which is able to form a local electric field. These differences in the charge in the different clusters of the surface have an influence on the transfer of the photogenerated $e'-h^*$ to the outside. At the (001) surface this charge separation process is from distorted $[WO_6]_d$ clusters to $[AgO_4 \cdot 3V_o^x]$, $[AgO_4 \cdot 2V_o^x]$ and $[AgO_5 \cdot 2V_o^x]$ undercoordinated clusters, while for the (101) surface, the e' donors are the distorted $[WO_6]_d$ clusters, in the third layer, and the e' acceptors are the $[WO_5 \cdot V_o^x]$ cluster in the first layer and the $[AgO_4 \cdot 3V_o^x]$ and $[AgO_5 \cdot 2V_o^x]$ clusters in the second layer.

34
35
36
37
38
39
40
41
42
43
44
45
46
47
48
49
50
51
52
53
54
55
56
57
58
59
60
61
62
63
64
65

The migrated e' can be trapped by the oxygen molecules, O_2 , adsorbed on the surface to generate O_2' radicals, while the h^* on the surface reacts with water molecules, H_2O , to yield OH^* and H^* radicals. Furthermore, these photogenerated ROS (O_2' and OH^* radicals) induce the antibacterial activity and degradation of RhB. These results indicate that the exposed surfaces of AWO can enhance the migration of photoinduced electrons, suppressing the recombination of charge carriers and improving the antibacterial and photocatalytic activity. Therefore, the undercoordinated and complete clusters at the surfaces $[AgO_y \cdot zV_o^x]$, and the distorted $[WO_6]_d$ and $[AgO_4]_d$, are the active sites capable of reacting with H_2O and O_2 , respectively, and can be considered the reservoirs of holes and electrons, respectively, as the active

1 sites in the antibacterial and photocatalytic activity. **Figure 6** shows a visual
2 representation of the main results obtained in this work. This mechanism
3 corresponds to an alternative and innovative point of view based on atomic-
4 level simulations used to describe the nature of the structural and electronic
5 properties associated with the presence of the exposed surfaces in the
6 morphology.
7
8
9
10
11
12
13
14
15
16
17
18
19
20
21
22
23
24
25
26
27
28
29
30
31
32
33
34
35
36
37
38
39
40
41
42
43
44
45
46
47
48
49
50
51
52
53
54
55
56
57
58
59
60
61
62
63
64
65

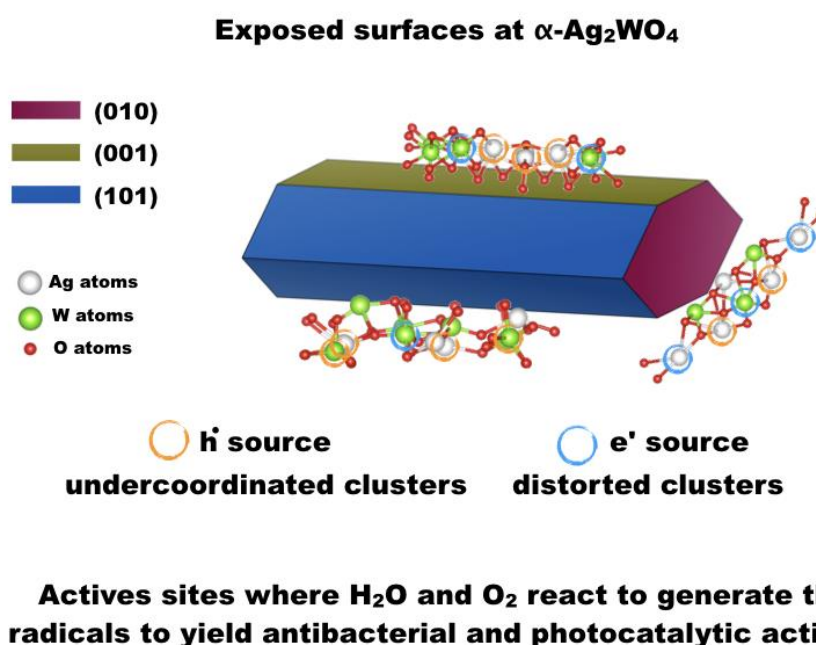


Figure 6. A visual representation of the main results obtained for the AWO microcrystals.

4 Conclusions

Semiconductor properties are controlled by the surfaces of their exposed crystals in the morphology and these effects can be understood through the analysis of their geometric and electronic structures with different local atomic coordination and band structure for the various surfaces. The new understandings of semiconductor materials are therefore extremely helpful to analyse experimental data from a more comprehensive perspective. An in-

1
2
3
4
5
6
7
8
9
10
11
12
13
14
15
16
17
18
19
20
21
22
23
24
25
26
27
28
29
30
31
32
33
34
35
36
37
38
39
40
41
42
43
44
45
46
47
48
49
50
51
52
53
54
55
56
57
58
59
60
61
62
63
64
65

depth characterization of the exposed surfaces remains a vital task for the development of the next generation of multifunctional materials.

In the present work, for the first time, the morphological evolution and the antibacterial and photocatalytic activity of AWO obtained by a CP method followed by microwave irradiation for different times have been systematically investigated and correlated with theoretical results from first-principles calculations. The performance and key electronic properties of an AWO semiconductor are dictated by the interplay between the surface structure and morphology, based on the analysis of the geometry and electronic properties of the exposed surfaces in the morphology. Our simulations revealed that there are two important factors that must be considered when investigating the surface electronic properties of AWO: first, the (001), (010) and (101) surfaces appear in all of the available morphologies that show enhanced antibacterial and photocatalytic activity, and second, the specific local coordination of the Ag and W cations in the exposed surface, i.e. the Ag and W clusters. In particular, we found that the stability of the surfaces and their electronic properties are correlated with the presence of incomplete $[AgO_y \cdot zV_O^x]$ and distorted $[WO_6]_d$ and $[AgO_4]_d$ clusters as the reservoirs of holes and electrons, respectively, which act as the active sites in the antibacterial and photocatalytic activity. Therefore, the as-synthesized AWO present a potent antibacterial effect against *Staphylococcus aureus*, and also show enhanced photocatalytic activity for the degradation of Rhodamine B. These subtle differences among the (001), (010) and (101) surfaces illustrate the influence of surface type on the reactivity. Controlling for the combination of surface types in the morphology thus provides an extremely sensitive tuning mechanism for the location of active sites.

1
2
3
4
5
6
7
8
9
10
11
12
13
14
15
16
17
18
19
20
21
22
23
24
25
26
27
28
29
30
31
32
33
34
35
36
37
38
39
40
41
42
43
44
45
46
47
48
49
50
51
52
53
54
55
56
57
58
59
60
61
62
63
64
65

This study introduces a new approach, based on the analysis, at the atomic level, of the exposed surfaces of the AWO to provide a deep understanding of the relationship between morphology, and antibacterial and photocatalytic activity. We considered the trade-off of activity versus stability for defective and rigorously optimized surfaces to identify patterns that are provably optimal. We have shown how to model general contributions to surface reactivity by using indicators for types of reactive sites. Overall, the approach involving the design of exposed surfaces via quantum mechanical calculation provides a new perspective in the design of highly efficient α -Ag₂WO₄ based materials. Our method is capable of establishing optimistic targets of material performance and can serve as a systematic guide for future efforts to synthesize other materials of interest.

Acknowledgements

This work was supported financially by Fundação de Amparo à Pesquisa do Estado de São Paulo (FAPESP 2013/07296-2, 2014/14171-4, 2017/13008-0, 2017/12594-3), Conselho Nacional de Desenvolvimento Científico e Tecnológico (CNPq 150949/2018-9). **J.A. acknowledges Universitat Jaume I for project, UJI-B2019-30, and Ministerio de Ciencia, Innovación y Universidades (Spain) project PGC2018-094417-B-I00 for supporting this research financially. We also wish to thank the Servei d'Informàtica, Universitat Jaume I, for their generous allocation of computer time. The valuable help of Lourdes Gracias from the UJI for the help in making calculations on the electronic structure and Enio Longo in improving the final versions of the figures is also acknowledged.**

1
2 **Conflict of Interest**
3

4 The authors declare no conflict of interest.
5
6

7
8 **ABBREVIATIONS**
9

10
11 ROS: Reactive Oxygen Species
12

13
14 DFT: Density Functional Theory
15

16
17 FE-SEM: Field Emission Scanning Electron Microscopy
18

19
20 XRD: X-ray Diffraction
21

22
23 PL: Photoluminescence
24

25
26 RhB: Rhodamine B
27

28
29 CP: Coprecipitation
30

31
32 UV-Vis: Ultraviolet-Visible
33

34
35 MR: Micro-Raman
36

37
38 BET: Brunauer–Emmett–Teller
39

40
41 ~~TSB: Tryptic Soy Broth~~
42

43
44 MIC: Minimum Inhibitory Concentration
45

46
47 MBC: Minimum Bactericidal Concentration
48

49
50 **ICSD**: Inorganic Crystal Structure Database
51

52
53 FWHM: Full Width at Half Maximum
54

55
56 VB: Valence Band
57

58
59 CB: Conduction Band
60

61
62 **CFU**: Colony Forming Unit
63

64
65 **Bibliography**

1. Tang J, Ye J (2005) Correlation of crystal structures and electronic structures and photocatalytic properties of the W-containing oxides. *J Mater Chem* 15:4246–4251. <https://doi.org/10.1039/B504818D>
2. da Silva LF, Catto AC, Avansi W, et al (2016) Acetone gas sensor based on α -Ag₂WO₄ nanorods obtained via a microwave-assisted hydrothermal route. *J Alloys Compd* 683:186–190. <https://doi.org/https://doi.org/10.1016/j.jallcom.2016.05.078>
3. Longo VM, De Foggi CC, Ferrer MM, et al (2014) Potentiated Electron Transference in α -Ag₂WO₄ Microcrystals with Ag Nanofilaments as Microbial Agent. *J Phys Chem A* 118:5769–5778. <https://doi.org/10.1021/jp410564p>
4. Longo E, Volanti DP, Longo VM, et al (2014) Toward an Understanding of the Growth of Ag Filaments on α -Ag₂WO₄ and Their Photoluminescent Properties: A Combined Experimental and Theoretical Study. *J Phys Chem C* 118:1229–1239. <https://doi.org/10.1021/jp408167v>
5. Foggi CC, Fabbro MT, Santos LPS, et al (2017) Synthesis and evaluation of α -Ag₂WO₄ as novel antifungal agent. *Chem Phys Lett* 674:125–129. <https://doi.org/https://doi.org/10.1016/j.cplett.2017.02.067>
6. Wang B-Y, Zhang G-Y, Cui G-W, et al (2019) Controllable fabrication of α -Ag₂WO₄ nanorod-clusters with superior simulated sunlight photocatalytic performance. *Inorg Chem Front* 6:209–219. <https://doi.org/10.1039/C8QI01025K>
7. Liu X, Hu J, Li J, et al (2013) Facile synthesis of Ag₂WO₄/AgCl nanorods for excellent photocatalytic properties. *Mater Lett* 91:129–132. <https://doi.org/https://doi.org/10.1016/j.matlet.2012.09.078>

- 1
2
3
4
5
6
7
8
9
10
11
12
13
14
15
16
17
18
19
20
21
22
23
24
25
26
27
28
29
30
31
32
33
34
35
36
37
38
39
40
41
42
43
44
45
46
47
48
49
50
51
52
53
54
55
56
57
58
59
60
61
62
63
64
65
8. Sreedevi A, Priyanka KP, Babitha KK, et al (2015) Chemical synthesis, structural characterization and optical properties of nanophase α - Ag_2WO_4 . *Indian J Phys* 89:889–897. <https://doi.org/10.1007/s12648-015-0664-1>
9. De Santana YVB, Gomes JEC, Matos L, et al (2014) Silver Molybdate and Silver Tungstate Nanocomposites with Enhanced Photoluminescence. *Nanomater Nanotechnol* 4:22. <https://doi.org/10.5772/58923>
10. Liang C, Guo H, Zhang L, et al (2019) Boosting molecular oxygen activation ability in self-assembled plasmonic pn semiconductor photocatalytic heterojunction of $\text{WO}_3/\text{Ag}@ \text{Ag}_2\text{O}$. *Chem Eng J* 372:12–25
11. Guo C-X, Yu B, Xie J-N, He L-N (2015) Silver tungstate: a single-component bifunctional catalyst for carboxylation of terminal alkynes with CO_2 in ambient conditions. *Green Chem* 17:474–479. <https://doi.org/10.1039/C4GC01638F>
12. Santos CJ, Moura Filho F, Campos FL, et al (2020) Ag_2WO_4 nanoparticles radiolabeled with technetium-99m: a potential new tool for tumor identification and uptake. *J Radioanal Nucl Chem* 323:51–59
13. Roca RA, Sczancoski JC, Nogueira IC, et al (2015) Facet-dependent photocatalytic and antibacterial properties of α - Ag_2WO_4 crystals: combining experimental data and theoretical insights. *Catal Sci Technol* 5:4091–4107. <https://doi.org/10.1039/C5CY00331H>
14. da Silva LF, Catto AC, Avansi W, et al (2014) A novel ozone gas sensor based on one-dimensional (1D) α - Ag_2WO_4 nanostructures. *Nanoscale* 6:4058–4062. <https://doi.org/10.1039/C3NR05837A>

- 1
2
3
4
5
6
7
8
9
10
11
12
13
14
15
16
17
18
19
20
21
22
23
24
25
26
27
28
29
30
31
32
33
34
35
36
37
38
39
40
41
42
43
44
45
46
47
48
49
50
51
52
53
54
55
56
57
58
59
60
61
62
63
64
65
15. Chen H, Xu Y (2014) Photoactivity and stability of Ag_2WO_4 for organic degradation in aqueous suspensions. *Appl Surf Sci* 319:319–323.
<https://doi.org/https://doi.org/10.1016/j.apsusc.2014.05.115>
16. Lin Z, Li J, Zheng Z, et al (2015) Electronic Reconstruction of $\alpha\text{-Ag}_2\text{WO}_4$ Nanorods for Visible-Light Photocatalysis. *ACS Nano* 9:7256–7265.
<https://doi.org/10.1021/acsnano.5b02077>
17. Wang X, Fu C, Wang P, et al (2013) Hierarchically porous metastable $\beta\text{-Ag}_2\text{WO}_4$ hollow nanospheres: controlled synthesis and high photocatalytic activity. *Nanotechnology* 24:165602. <https://doi.org/10.1088/0957-4484/24/16/165602>
18. Xu D, Cheng B, Zhang J, et al (2015) Photocatalytic activity of Ag_2MO_4 (M = Cr, Mo, W) photocatalysts. *J Mater Chem A* 3:20153–20166.
<https://doi.org/10.1039/C5TA05248C>
19. Golubović A, Šćepanović M, Kremenović A, et al (2008) Raman study of the variation in anatase structure of TiO_2 nanopowders due to the changes of sol–gel synthesis conditions. *J Sol-Gel Sci Technol* 49:311.
<https://doi.org/10.1007/s10971-008-1872-3>
20. Sreedevi A, Priyanka KP, Vattappalam SC, Varghese T (2018) Silver Tungstate Nanoparticles for the Detection of Ethanol, Ammonia and Acetone Gases. *J Electron Mater* 47:6328–6333.
<https://doi.org/10.1007/s11664-018-6551-8>
21. Macedo NG, Gouveia AF, Roca RA, et al (2018) Surfactant-Mediated Morphology and Photocatalytic Activity of $\alpha\text{-Ag}_2\text{WO}_4$ Material. *J Phys Chem C* 122:8667–8679. <https://doi.org/10.1021/acs.jpcc.8b01898>
22. Dutta DP, Singh A, Ballal A, Tyagi AK (2014) High Adsorption Capacity

1 for Cationic Dye Removal and Antibacterial Properties of Sonochemically
2 Synthesized Ag_2WO_4 Nanorods. Eur J Inorg Chem 2014:5724–5732.

3
4
5 <https://doi.org/10.1002/ejic.201402612>

- 6
7 23. Sofi FA, Majid K (2019) Plasmon induced interfacial charge transfer
8 across Zr-based metal-organic framework coupled Ag_2WO_4
9 heterojunction functionalized by Ag NPs: Efficient visible light
10 photocatalyst. Chem Phys Lett 720:7–14.
11
12 <https://doi.org/https://doi.org/10.1016/j.cplett.2019.02.005>
- 13
14 24. Pan L, Li L, Chen Y (2013) Synthesis and electrocatalytic properties of
15 microsized Ag_2WO_4 and nanoscaled MWO_4 (M=Co, Mn). J Sol-Gel Sci
16 Technol 66:330–336. <https://doi.org/10.1007/s10971-013-3014-9>
- 17
18 25. Nobre FX, Bastos IS, dos Santos Fontenelle RO, et al (2019)
19 Antimicrobial properties of $\alpha\text{-Ag}_2\text{WO}_4$ rod-like microcrystals synthesized
20 by sonochemistry and sonochemistry followed by hydrothermal
21 conventional method. Ultrason Sonochem 58:104620.
22
23 <https://doi.org/https://doi.org/10.1016/j.ultsonch.2019.104620>
- 24
25 26. Cheng L, Shao Q, Shao M, et al (2009) Photoswitches of One-
26 Dimensional Ag_2MO_4 (M = Cr, Mo, and W). J Phys Chem C 113:1764–
27 1768. <https://doi.org/10.1021/jp808907e>
- 28
29 27. Cavalcante LS, Almeida MAP, Avansi W, et al (2012) Cluster
30 Coordination and Photoluminescence Properties of $\alpha\text{-Ag}_2\text{WO}_4$
31 Microcrystals. Inorg Chem 51:10675–10687.
32
33 <https://doi.org/10.1021/ic300948n>
- 34
35 28. Andrés J, Gracia L, Gonzalez-Navarrete P, et al (2014) Structural and
36 electronic analysis of the atomic scale nucleation of Ag on $\alpha\text{-Ag}_2\text{WO}_4$
37
38
39
40
41
42
43
44
45
46
47
48
49
50
51
52
53
54
55
56
57
58
59
60
61
62
63
64
65

1 induced by electron irradiation. Sci Rep 4:5391

- 2
3
4
5
6
7
8
9
10
11
12
13
14
15
16
17
18
19
20
21
22
23
24
25
26
27
28
29
30
31
32
33
34
35
36
37
38
39
40
41
42
43
44
45
46
47
48
49
50
51
52
53
54
55
56
57
58
59
60
61
62
63
64
65
29. Longo E, Cavalcante LS, Volanti DP, et al (2013) Direct in situ observation of the electron-driven synthesis of Ag filaments on α -Ag₂WO₄ crystals. Sci Rep 3:1676
30. de Foggi CC, de Oliveira RC, Fabbro MT, et al (2017) Tuning the Morphological, Optical, and Antimicrobial Properties of α -Ag₂WO₄ Microcrystals Using Different Solvents. Cryst Growth Des 17:6239–6246. <https://doi.org/10.1021/acs.cgd.7b00786>
31. Beg MA, Jain A (1992) Kinetics and mechanism of reactions of silver tungstate with mercuric bromiodide and mercuric chlorobromide in the solid state. Polyhedron 11:2775–2780. [https://doi.org/https://doi.org/10.1016/S0277-5387\(00\)83635-9](https://doi.org/https://doi.org/10.1016/S0277-5387(00)83635-9)
32. Pereira PFS, Nogueira IC, Longo E, et al (2015) Rietveld refinement and optical properties of SrWO₄: Eu³⁺ powders prepared by the non-hydrolytic sol-gel method. J Rare Earths 33:113–128
33. Yu S-H, Liu B, Mo M-S, et al (2003) General Synthesis of Single-Crystal Tungstate Nanorods/Nanowires: A Facile, Low-Temperature Solution Approach. Adv Funct Mater 13:639–647. <https://doi.org/10.1002/adfm.200304373>
34. Cui X, Yu S-H, Li L, et al (2004) Selective Synthesis and Characterization of Single-Crystal Silver Molybdate/Tungstate Nanowires by a Hydrothermal Process. Chem – A Eur J 10:218–223. <https://doi.org/10.1002/chem.200305429>
35. Ondruschka B, Bonrath W, Stuerger D (2012) In Microwaves in Organic Synthesis, Vol. 1; de la Hoz, A.; Loupy, A., Eds.

- 1
2
3
4
5
6
7
8
9
10
11
12
13
14
15
16
17
18
19
20
21
22
23
24
25
26
27
28
29
30
31
32
33
34
35
36
37
38
39
40
41
42
43
44
45
46
47
48
49
50
51
52
53
54
55
56
57
58
59
60
61
62
63
64
65
36. Kappe CO (2013) How to measure reaction temperature in microwave-heated transformations. *Chem Soc Rev* 42:4977–4990.
<https://doi.org/10.1039/C3CS00010A>
 37. Kappe CO, Pieber B, Dallinger D (2013) Microwave Effects in Organic Synthesis: Myth or Reality? *Angew Chemie Int Ed* 52:1088–1094.
<https://doi.org/10.1002/anie.201204103>
 38. Polshettiwar V, Varma RS (2010) Green chemistry by nano-catalysis. *Green Chem* 12:743–754. <https://doi.org/10.1039/B921171C>
 39. Bilecka I, Niederberger M (2010) Microwave chemistry for inorganic nanomaterials synthesis. *Nanoscale* 2:1358–1374.
<https://doi.org/10.1039/B9NR00377K>
 40. Macario LR, Moreira ML, Andrés J, Longo E (2010) An efficient microwave-assisted hydrothermal synthesis of BaZrO₃ microcrystals: growth mechanism and photoluminescence emissions. *CrystEngComm* 12:3612–3619. <https://doi.org/10.1039/C004034G>
 41. Pereira PFS, Gouveia AF, Assis M, et al (2018) ZnWO₄ nanocrystals: synthesis, morphology, photoluminescence and photocatalytic properties. *Phys Chem Chem Phys* 20:1923–1937.
<https://doi.org/10.1039/C7CP07354B>
 42. Ebadi M, Mat-Teridi MA, Sulaiman MY, et al (2015) Electrodeposited p-type Co₃O₄ with high photoelectrochemical performance in aqueous medium. *RSC Adv* 5:36820–36827. <https://doi.org/10.1039/C5RA04008F>
 43. Andrés J, Gracia L, Gouveia AF, et al (2015) Effects of surface stability on the morphological transformation of metals and metal oxides as investigated by first-principles calculations. *Nanotechnology* 26:405703.

<https://doi.org/10.1088/0957-4484/26/40/405703>

- 1
2
3
4
5
6
7
8
9
10
11
12
13
14
15
16
17
18
19
20
21
22
23
24
25
26
27
28
29
30
31
32
33
34
35
36
37
38
39
40
41
42
43
44
45
46
47
48
49
50
51
52
53
54
55
56
57
58
59
60
61
62
63
64
65
44. Fabbro MT, Saliby C, Rios LR, et al (2015) Identifying and rationalizing the morphological, structural, and optical properties of β -Ag₂MoO₄ microcrystals, and the formation process of Ag nanoparticles on their surfaces: combining experimental data and first-principles calculations. *Sci Technol Adv Mater* 16:65002. <https://doi.org/10.1088/1468-6996/16/6/065002>
45. Bomio MRD, Tranquilin RL, Motta F V, et al (2013) Toward Understanding the Photocatalytic Activity of PbMoO₄ Powders with Predominant (111), (100), (011), and (110) Facets. A Combined Experimental and Theoretical Study. *J Phys Chem C* 117:21382–21395. <https://doi.org/10.1021/jp407416h>
46. Lu JJ, Ulrich J (2005) The influence of supersaturation on crystal morphology – experimental and theoretical study. *Cryst Res Technol* 40:839–846. <https://doi.org/10.1002/crat.200410443>
47. Longo VM, Gracia L, Stroppa DG, et al (2011) A Joint Experimental and Theoretical Study on the Nanomorphology of CaWO₄ Crystals. *J Phys Chem C* 115:20113–20119. <https://doi.org/10.1021/jp205764s>
48. Botelho G, Andres J, Gracia L, et al (2016) Photoluminescence and Photocatalytic Properties of Ag₃PO₄ Microcrystals: An Experimental and Theoretical Investigation. *Chempluschem* 81:202–212. <https://doi.org/10.1002/cplu.201500485>
49. Oliveira MC, Gracia L, Nogueira IC, et al (2016) Synthesis and morphological transformation of BaWO₄ crystals: Experimental and theoretical insights. *Ceram Int* 42:10913–10921.

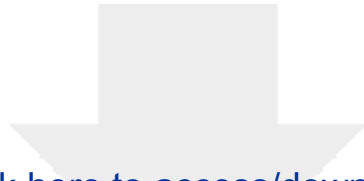
<https://doi.org/https://doi.org/10.1016/j.ceramint.2016.03.225>

- 1
2
3
4
5
6
7
8
9
10
11
12
13
14
15
16
17
18
19
20
21
22
23
24
25
26
27
28
29
30
31
32
33
34
35
36
37
38
39
40
41
42
43
44
45
46
47
48
49
50
51
52
53
54
55
56
57
58
59
60
61
62
63
64
65
50. Silva GS, Gracia L, Fabbro MT, et al (2016) Theoretical and Experimental Insight on Ag_2CrO_4 Microcrystals: Synthesis, Characterization, and Photoluminescence Properties. *Inorg Chem* 55:8961–8970.
<https://doi.org/10.1021/acs.inorgchem.6b01452>
51. Gouveia AF, Ferrer MM, Sambrano JR, et al (2016) Modeling the atomic-scale structure, stability, and morphological transformations in the tetragonal phase of LaVO_4 . *Chem Phys Lett* 660:87–92.
<https://doi.org/https://doi.org/10.1016/j.cplett.2016.08.013>
52. Gao Z, Sun W, Hu Y (2014) Mineral cleavage nature and surface energy: Anisotropic surface broken bonds consideration. *Trans Nonferrous Met Soc China* 24:2930–2937. [https://doi.org/https://doi.org/10.1016/S1003-6326\(14\)63428-2](https://doi.org/https://doi.org/10.1016/S1003-6326(14)63428-2)
53. Gao H, Zheng C, Yang H, et al (2019) Construction of a CQDs/ Ag_3PO_4 / BiPO_4 heterostructure photocatalyst with enhanced photocatalytic degradation of rhodamine B under simulated solar irradiation. *Micromachines* 10:557
54. Ferrer MM, Gouveia AF, Gracia L, et al (2016) A 3D platform for the morphology modulation of materials: first principles calculations on the thermodynamic stability and surface structure of metal oxides: Co_3O_4 , α - Fe_2O_3 , and In_2O_3 . *Model Simul Mater Sci Eng* 24:25007.
<https://doi.org/10.1088/0965-0393/24/2/025007>
55. Standarts N (2007) Clinical and Laboratory Standards Institute, Methods for dilution antimicrobial susceptibility tests for bacteria that grow aerobically; approved standard, CLSI document M7-A7. *Clin Lab Stand*

Institute, Wayne, PA

- 1
2
3
4
5
6
7
8
9
10
11
12
13
14
15
16
17
18
19
20
21
22
23
24
25
26
27
28
29
30
31
32
33
34
35
36
37
38
39
40
41
42
43
44
45
46
47
48
49
50
51
52
53
54
55
56
57
58
59
60
61
62
63
64
65
56. Machado TR, Macedo NG, Assis M, et al (2018) From Complex Inorganic Oxides to Ag–Bi Nanoalloy: Synthesis by Femtosecond Laser Irradiation. ACS omega 3:9880–9887
57. Roca RA, Sczancoski JC, Nogueira IC, et al (2015) Facet-dependent photocatalytic and antibacterial properties of α -Ag₂WO₄ crystals: combining experimental data and theoretical insights. Catal Sci Technol 5:4091–4107. <https://doi.org/10.1039/C5CY00331H>
58. Kröger FA, Vink HJ (1956) Relations between the Concentrations of Imperfections in Crystalline Solids. In: Seitz F, Turnbull DBT-SSP (eds). Academic Press, pp 307–435
59. Gouveia AF, Assis M, Cavalcante LS, et al (2018) Reading at exposed surfaces: theoretical insights into photocatalytic activity of ZnWO₄. Front Res Today 1:1005. <https://doi.org/10.31716/frt.201801005>
60. Assis M, Cordoncillo E, Torres-Mendieta R, et al (2018) Towards the scale-up of the formation of nanoparticles on α -Ag₂WO₄ with bactericidal properties by femtosecond laser irradiation. Sci Rep 8:1884. <https://doi.org/10.1038/s41598-018-19270-9>
61. Macedo NG, Machado TR, Roca RA, et al (2019) Tailoring the bactericidal activity of Ag nanoparticles/ α -Ag₂WO₄ composite induced by electron beam and femtosecond laser irradiation: Integration of experiment and computational modeling. ACS Appl Bio Mater 2:824–837
62. Wang QP, Guo XX, Wu WH, Liu SX (2011) Preparation of fine Ag₂WO₄ antibacterial powders and its application in the sanitary ceramics. In: Advanced Materials Research. Trans Tech Publ, pp 1321–1325

- 1
2
3
4
5
6
7
8
9
10
11
12
13
14
15
16
17
18
19
20
21
22
23
24
25
26
27
28
29
30
31
32
33
34
35
36
37
38
39
40
41
42
43
44
45
46
47
48
49
50
51
52
53
54
55
56
57
58
59
60
61
62
63
64
65
63. Moura JVB, Freitas TS, Cruz RP, et al (2017) β -Ag₂MoO₄ microcrystals: Characterization, antibacterial properties and modulation analysis of antibiotic activity. *Biomed Pharmacother* 86:242–247
 64. Long R, Huang H, Li Y, et al (2015) Palladium-Based Nanomaterials: A Platform to Produce Reactive Oxygen Species for Catalyzing Oxidation Reactions. *Adv Mater* 27:7025–7042
 65. Akter M, Sikder MT, Rahman MM, et al (2018) A systematic review on silver nanoparticles-induced cytotoxicity: Physicochemical properties and perspectives. *J Adv Res* 9:1–16
 66. Gold K, Slay B, Knackstedt M, Gaharwar AK (2018) Antimicrobial Activity of Metal and Metal-Oxide Based Nanoparticles. *Adv Ther* 1:1700033
 67. Gouveia AF, Sczancoski JC, Ferrer MM, et al (2014) Experimental and Theoretical Investigations of Electronic Structure and Photoluminescence Properties of β -Ag₂MoO₄ Microcrystals. *Inorg Chem* 53:5589–5599.
<https://doi.org/10.1021/ic500335x>
 68. Zhang C, Zhang H, Zhang K, et al (2014) Photocatalytic Activity of ZnWO₄: Band Structure, Morphology and Surface Modification. *ACS Appl Mater Interfaces* 6:14423–14432. <https://doi.org/10.1021/am503696b>



[Click here to access/download](#)

Electronic Supplementary Material
Supplementary Information 20.05.2020.docx

